Analysis of sea ice concentration and thickness over Barents Sea using standard logistic curve model

Dency V. Panicker[1], Bhasha Vachharajani[1]*, Rohit Srivastava[1] and Sandip R. Oza[2]
[1]Pandit Deendayal Energy University, Gandhinagar, Gujarat, INDIA
[2]Space Applications Centre, ISRO, Ahmedabad, Gujarat, INDIA
*Email: bhasha.vachharajani@sot.pdpu.ac.in

(Received: 2nd September 2022, Accepted in final form: 19 March 2023)

DOI: *https://doi.org/10.58825/jog.2023.17.1.74*

Abstract: As marginal, the Barents Sea plays a major role in the process of Atlantification, and large seasonal variability in sea ice is observed over the region. Current sea ice concentration and thickness obtained from satellite help one understand the variation in sea ice is seasonal. During summer, the concentration and thickness of sea ice are seen to fall, and during winters, it is seen to rise. In order to understand the difference in these variabilities and to analyse the future state of sea ice, a standard logistic curve model is considered. The standard logistic curve model is applied to sea ice parameters during summer and winter to quantify the sea ice growth and decay processes over the Barents Sea.The model yields predicted values based on the adjustment parameter (b) used.Results show that the predicted sea ice concentration performs well with the satellite sea ice concentration values. The model is run on the timeframe grouped into two, with each set having an average of ten years from 2000-2020. For the decay process, the fitted sea ice concentration decay curves derived from the standard logistic curve model are in good agreement with the observed data for the two timelines, with r^2 = 0.88 and 0.87, respectively. Similarly, for the growth process, the relevant fitted decay curves derived from the standard logistic curve model are also in good agreement with the observed data during the above different time periods withr^2= 0.80 and 0.78, respectively. Further, the model is implied to sea ice thickness, and the result obtained by the logistic curve model is found to be consistent with the satellite sea ice thickness with r^2 = 0.75 for the years 2011–2020. Particularly, both the rapid sea ice increase pattern during the growth process and the remarkable decrease pattern during the decay process are successfully characterized by the corresponding fitted curves. The introduction of calculated adjustment parameters into the model helps in accurately determining the sea ice variables, which brings us closer to conservation tools that mitigate therisks associated with rapid sea ice loss.

Keywords: Sea ice concentration, Sea ice thickness, Barents Sea, Logistic curve model, Growth process, Decay process

1. Introduction

Earth's overall temperature warmed by 0.8 °C (Intergovernmental Panel on Climate Change, 2018) since the late 19th century, while the Arctic has warmed by 2 - 3 °C over the same span (Allen et al., 2018). Similarly, Antarctica, the coldest, windiest, and driest continent on Earth, has also experienced prominent decadal and interannual variation in mean annual temperature anomalies. The increase in temperature has caused a total ice sheet loss (Turner et al., 2019) from 40 ± 9 Gt/y in 1979–1990 (Schröder et al., 2018) to 252 ± 26 Gt/y in 2009–2017 (e.g., King & Turner, 1997). With an increase in temperature, pronounced seasonality, and the year-round presence of ice and snow, the Arctic and Antarctica may face different futures in response to topographical and geographical reasons (Meredith et al., 2019). The temperature hike due to warming is of great concern as the poles are important components of the global climate system and their changes have highly impacted ocean hydrology, atmospheric circulation, and climate change (Kim et al., 2014). Overall, one of the most visible signs of warming changes over the poles is the declining sea ice cover. Sea ice concentration and extent, which are clear indicators of sea ice cover, have decreased in all months over the past 30 years (Parkinson, 2019). Particularly during summer, the sea ice is seen to be thinning. As the thinner ice dominates the thicker ice, the younger ice type is seen to be more prevalent than the multiyear ice (Meier et al., 2014).

Due to the diverging nature (decline in sea ice occurs at different rates in different regions and seasons) of the Arctic, unlike the Antarctic in terms of its ocean influence, many scientists have projected the Arctic to be ice-free in most late summers as soon as the 2030s (Wang et al., 2009; Holland et al., 2006; Boé et al., 2010; Eisenman & Wettlaufer, 2008; Notz et al., 2009). The future of Arctic sea ice cover is of enormous climatic and economic significance (ACIA, 2005). The daily sea ice concentration data from the NSIDC shows that the sea ice concentration varies significantly between 2007 and 2012. The maximum (higher) values of sea ice concentration was reducing, while the minimum (lower) values of concentration were found to be increasing (Vázquez et al., 2016). The highest decreasing rates are mainly focused on the Beaufort, Chukchi, and East Siberian Seas (Chen & Zhao, 2017; Zhao et al., 2017). In the summer of 2010, there was a very low sea ice concentration (30%) that appeared at high Arctic latitudes, even lower than that of the surrounding pack of ice at lower latitudes (Cavalieri & Parkinson, 2012). The extent of perennial sea ice in the Arctic decreased rapidly, and in the East Arctic Ocean, it continued to be depleted

with area-wise reduction of 70% from October 2005 to April 2006 (Nghiem et al., 2006). Along with concentration and extent, sea ice thickness is another key characteristic of the sea ice cover. Sea ice that are thick enough can survive the summer melt season and may last for many years. For ice to thicken, the ocean must lose heat to the atmosphere. But this thicker sea ice deteriorates the coupling between the ocean and atmosphere systems (Vella & Wettlaufer, 2008). Thicker sea ice is a strong thermal insulator; as a result, it limits heat transfer from the ocean to the atmosphere in winter and also its thermodynamic growth (Petty et al., 2018; Rösel et al., 2018). By the end of winters, thicker ice gets developed, decreasing the transmission of solar radiation to the surface ocean and reducing the potential primary productivity (Mundy et al., 2005; Katlein et al., 2015). Also, this thick sea ice is more likely to survive the melt season, increasing the average age of sea ice.

While investigating the influence of oceans over sea ice, the Barents Sea is found to be a hotspot for Arctic climate change (King et al., 2017; Lind et al., 2018; Schlichtholz, 2019; Skagseth et al., 2020), with pronounced upper ocean warming and a retreating sea ice cover over the past two decades (Sorokina et al., 2016; Screen et al., 2018). The Barents Sea is one of the marginal shelf seas of the Arctic Ocean, which surrounds the Arctic Basin. The sea is located in the European sector of the Arctic and is influenced by both Atlantic and Arctic waters. Most of the sea ice in the Barents Sea is formed locally, with a fraction imported from the Arctic Basin through the straits between Svalbard and Novaya Zemlya. The marginal ice zone in the western Barents Sea extends south to 75 -78° N in early spring and retreats to about 80-82° N in late summer. This trend has been seen extending to higher latitudes during the last 10 years (Tronstad et al., 2007). It is expected that ice cover in the Barents Sea will continue to reduce in the future also due to (i) increase in Arctic air temperature, (ii) recent increase of cyclonic activity in northern north Atlantic and associated ocean heat anomalies, and (iii) depletion of sea ice in the eastern Arctic Ocean and thus less import of thick ice into the Barents Sea region (Smedsrud et al., 2013). Additionally, air-sea temperature differences in the Barents Sea are extremely large, ocean heat release reaches values of 300-500 Wm^{-2} (Simonsen and Haugan, 1996). The Barents Sea dominates the seasonal Arctic heat budget and has the most vigorous ocean air exchange in the Arctic, making it a centre of influence on the high latitude climate system (Serreze et al., 2007). Studies suggest that the decrease in sea ice over the Barents Sea in early winter also affects cyclonic pathways in the downstream region (Inoue et al., 2012) and results in a warm Arctic pattern. The Barents Sea ice extent in winter has decreased since 1850 (Shapiro et al., 2003), and the retreat observed during recent decades has been the largest decrease in the Arctic (Parkinson & Cavalieri, 2008).

The decline in sea ice is faster than what most models have forecasted, leading to possible near-ice-free summer conditions in the coming decades. This is due to a combination of factors, including the complexity of the Arctic climate system and the difficulty of modeling the interactions between different components of the system (Walsh et al., 2017). Most climate models have predicted a decline in Arctic sea ice extent and thickness in response to increasing greenhouse gas concentrations in the atmosphere. However, the actual decline has been more rapid than what the models have projected. For example, the minimum Arctic sea ice extent in September 2020 was the second-lowest on record (Diebold et al., 2020), despite most models predicting that such low extents would not be reached until the 2030s. According to climate change experiments based on phase 5 of the Climate Model Intercomparison Project (CMIP5), the warm Arctic anomalies will continue in the future (Yang and Christensen, 2012). Additionally, a new generation of atmosphere-ocean coupled reanalysis, the National Centers for Environmental Prediction Climate Forecast System Reanalysis (NCEP CFSR), has been produced. The NCEP CFSR has benefited from advances in operational weather forecasting and previous reanalysis improvements (Bengtsson et al., 2007). The NCEP CFSR assimilates the oceanic field, including sea ice concentration. Therefore, it is expected that the predictability of the sea ice and its relation to the atmosphere and ocean variability can be examined. Similar to such models, is the Community Earth System Model (CESM), which is used to simulate the interactions between the atmosphere, oceans, land surface, and sea ice. It is used to make projections of future sea ice conditions under different climate scenarios (Danabasoglu et al., 2020). For short-term (daily to seasonal) timescale prediction, the Arctic Regional Ocean Model (AROM) is generally used (Ren et al., 2021). The Pan-Arctic Ice-Ocean Modeling and Assimilation System (PIOMAS) is used to track changes in Arctic sea ice over time and make predictions about future sea ice conditions (Zhang and Rothrock, 2003). These models are continually being refined and improved as more data becomes available and our understanding of the complex processes that govern sea ice behaviour increases. Similar to these models, one such model that can help in assessing the growth and future of sea ice conditions is the standard logistic curve model (Hui, 2006). This model had been used originally to analyse the growth of population, where the carrying capacity denoted the population size at which the population growth rate equals zero. But now, the model is being used in various fields of science (Meyer, 1994). As the model made space in every aspect of science (Bony et al., 2006), the carrying capacity now represented merely the value of a state variable at which its growth rate equals zero in a system. Researchers in the past have used this logistic curve model to understand the sea ice conditions over Antarctica (Tietsche et al., 2013) and Arctic (Bitz and Lipscomb, 1999). Over the Arctic, the model was used to study the seasonal cycle of Arctic sea ice volume.

The paper illustrates and discusses the use of the standard logistic curve model to understand the behaviour of sea ice during summers and winters. This study aims to explore and characterize a quantitative statistical model in order to better quantify and simulate the sea ice growth and decay processes in the Barents Sea during 2000-

2020. The paper aims to study sea ice concentration and sea ice thickness, obtained through the model, to analyse how the sea behaves during various seasons; summer and winter. Here, the evolution of sea ice over the region, that is, from the freeze onset to its maximum attainment, is considered. These parameters further help in projecting the future of the Arctic sea ice. The model operates based on the threshold value allotted to the adjustment parameter. The model can operate on two types of adjustment parameters: one by fixing it and the other by varying it. Here the major goal revolves around finding which value of the adjustment parameter can better fit with the satellite sea ice values, therefore offering an opportunity for predicting sea ice state on seasonal timescales. The current model aims at providing valuable information on how sea ice parameters evolve and how it will be affected by changing climate. This model can be used for long-term climate studies, short-term operational forecasts (within the duration of one year or so), and seasonal forecasts (such as during the decay and growth phases of sea ice).

2. Datasets and Methodology

For the current study, consistent monthly sea ice concentration (SIC) and sea ice thickness (SIT), of the Barents Sea of the Arctic region are considered.

2.1 Datasets

SIC data is selected from National Snow and Ice Data Center (NSIDC) (Stroeve et al., 2018) for the years 2000-2020. The spatial resolution of the data is 0.22° x 0.22°. The SIC data is retrieved based on the NASA TEAM algorithm in terms of the brightness temperature data. The accuracy of total sea ice concentration is within ± 5 % of the actual sea ice concentration in winter, and ± 15 % in the Arctic during summer when melt ponds are present on the sea ice. Accuracy tends to be best within the consolidated ice pack when the sea ice is relatively thick and ice concentration is high. Accuracy decreases as the proportion of thin ice increases (Cavalieri et al., 1996). However as the time range considered for this study is limited to just 20 years, such a decline in accuracy is irrelevant in the current case. Additionally, SIT data have also been taken from NSIDC (Kurtz and Harbeck, 2017) CryoSat-2, but for the span of 2010-2020. The spatial resolution of the SIT data is 0.22° x 0.22°. The CryoSat-2 data set contains estimates of Arctic Sea ice thickness and SIC, ice freeboard and surface roughness, as well as snow density and depth, derived from the ESA CryoSat-2 Synthetic Aperture Interferometric Radar Altimeter (SIRAL). Quality assessment of this data is done through comparison with NASA's Operation IceBridge data. Freeboard error for a 0.22° grid cell from the associated surface elevation retrieval error is estimated as ±0.065 m in comparison with IceBridge data (Kurtz and Harbeck, 2017). The shape files for the Barents Sea are extracted from Marine Regions Database. Marine Regions are generally used to create a standard, relational list of geographic names, coupled with information and maps of the geographic location of these features.

2.2 Methodology

To understand the state of sea ice prevailing over the region, satellite-observed monthly SIC and SIT are considered. After the extraction of these datasets from the aforementioned sources, they are put through pre-processing. The data is pre-processed to extract the cryospheric variables, latitudes, and longitudes. The data is further re-projected into a different coordinate system (npstere-north polar stereographic projection) corresponding to the spatial resolutions of both the datasets. Firstly, the spatio-temporal analysis of SIC is carried out. For the spatial analysis, the years 2000–2004 were considered as the background years from which the averages of 2005–2009, 2010–2014, and 2015–2019 were subtracted. The maps of the long-term average 2000–2004 SIC from 2005–2009, 2010–2014, and 2015–2019 at each location for each month were generated. However, the variability in SIC for the month of December, January, February, and March is displayed and thoroughly discussed in the upcoming section. For temporal variation of the parameter, monthly whisker plots are generated. Here, each month is represented as a box with whiskers extending the minimum and maximum values. The median is shown by a horizontal line inside the box, and the quartiles by a vertical line inside the box. Lastly, SIT is also analysed across the domain in a similar manner. The only difference between the two analyses is that SIC is carried out for all the months of the year, whereas SIT is only performed for the winter months due to the lack of availability of SIT data during the summer months. Further, SIC and SIT during the winter months, specifically January, February and March are intensely examined. Histograms with bins are considered for the ease of understanding. SIC is averaged over Barents Sea for the entire span of each month. The binning technique is used to reduce the amount of data. By using the trial-and-error method, a suitable bin size of 70 was found, which removed the insignificant lower values and helped in the representation of the growth of SIC. The selected bin size clearly depicted the intensification of SIC from lower values to higher concentrations. However, for SIT, along with the knowledge of the number of pixels lying within a particular thickness, Gaussian density plots are also extracted. In the case of SIT, the Gaussian distribution gave a better understanding as it shows the continuous distribution of data around its center. Additionally, here the mean, median and mode are equal, giving a better knowledge of the shift in the variable during each month. Furthermore, for the quantitative analysis of the variability of sea ice, the logistic growth model is used to understand the seasonal sea ice growth and decay over the Barents Sea. For better clarity and transparency of the research methodology adopted in the paper, a flow chart is illustrated in Figure 1. The logistic curve model mentioned in the flow chart, used to predict the cryospheric parameters (SIC and SIT) is elaborately explained in Section 2.2.1.

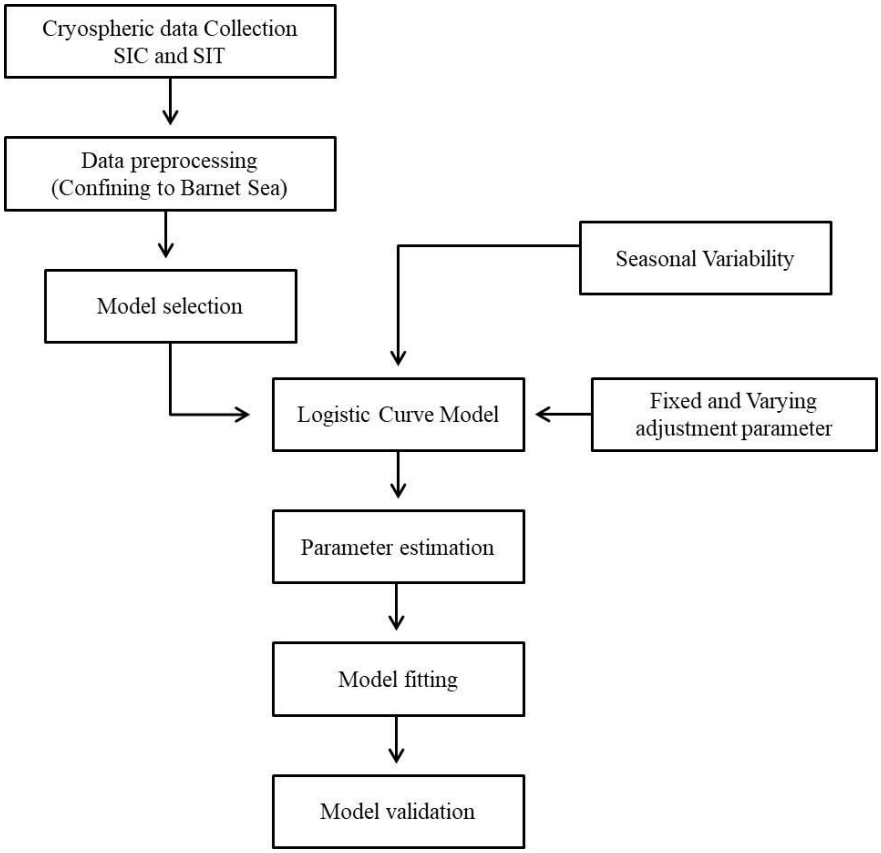

Figure 1. Flow chart describing the methodology used

2.2.1 Standard logistic curve model

In 1838, the Logistic function was first proposed by Pierre François Verhulst in the context of population growth. Verhulst derived the logistic equation to describe the growth of the biological population (Kyurkchiev and Markov, 2015). Interestingly, Sweilam et al. (2012) assert that the logistic equation is described by a first-order ordinary differential equation. Their study resonates further with Murphy et al., 2016 who noted that the logistic equation is formalized by the differential equation. Later various modifications were made to the function to fit into various spheres of science. The mathematical equation of the standard logistic curve model is as follows:

$$Y = \frac{L}{1+be^{-kt}} \quad (1)$$

In Eq. (1), 'Y' refers to the observed temporal SIC or SIT at any month (t), 'L' is the carrying capacity (in summers it is seen varying but, during winters as the Arctic region is completely frozen, L = 100% for SIC and L = 3 m for SIT), 'b' stands for the adjustment parameter, which is to be calculated from the existing parameter value given, 'e' refers to the natural logarithm base, and 'k' represents the Logistic growth rate at which the ice concentration/thickness approaches L. This model has the ability to describe the growth stage, such as formation, development, maturity, and limit, of sea ice. The carrying capacity is determined by calculating the maximum occurrences of the highest value of SIC and SIT obtained over any pixel in the Barents Sea during winter and summer in the background years (2000–2004). During winter (October–March), SIC is found to have maximum value of 100% in 2000–2004, whereas during summer (April-September), L=87%. Similarly for SIT, L = 3 m during winters. Here, only the winter season is considered, as this dataset is unavailable during summer months.

During winter the equation for SIC becomes:

$$Y = \frac{100}{1+be^{-kt}} \quad (2)$$

And for summers the equation is, simplified as:

$$Y = \frac{87}{1+be^{-kt}} \quad (3)$$

For SIT, eq. (1) becomes:

$$Y = \frac{3}{1+be^{-kt}} \quad (4)$$

Using these equations, the values of b and k are calculated for each season. Further, in order to evaluate the performance of the model, statistical methods, viz., regression analyses, are performed which aid in computing its slope, intercepts, standard error, and p-value.

3. Results and discussion

3.1 Spatio-temporal variations of monthly SIC over Barents Sea

The two decades 2000–2010 and 2010–2020 are divided into four lustrums: 2001–2005, 2006–2010, 2011–2015, and 2016–2020. The first five years are considered to be the base (background years), and the other successive three sets of five years are compared with it to understand the deviation of sea ice conditions from its initial stage. Or, in other words, anomalies in all the latter three sets are found by comparing them with the average of the former span (2001–2005). Values below zero indicate that the present duration consists of more SIC than the base duration. If the values are positive (above zero), the current period could not build more SIC compared to the base. In the case of October, November, and December, the period is divided into 2000–2004, 2005–2009, 2010–2014, and 2015–2019. This is done so as to place October-December first in every winter season (for example, the timeline is taken as October 2000, November 2000, December 2000, January 2001, February 2001, and March 2001). Analyses have been carried out for all the months; however, spatial maps of SIC during December, January, February, and March are displayed in Figure 2.

During December, the contrast is predominantly found over the Barents Sea. The regions above and east of Svalbard greatly experience a disparity. The difference indicates that during 2005–2009 (Figure 2a), the sea lost immense ice. This significant variation is also found above and to the east of Novaya Zemlya. As we move towards the right, as shown in the subsequent plots, it is clearly observed that the deviation has built up. The regions around Svalbard and portions below Franz Josef have highly lost sea ice during the time span of 2010–2014 (Figure 2b). Apart from the Barents Sea, the difference is observed over the Kara and White Seas. During 2015–2019 (Figure 2c), the sea again failed to recover its lost sea ice conditions, making the contrast appear more intense. The Arctic Circle and the region near Svalbard also show a positive anomaly. December is an important month in the life cycle of Arctic sea ice in general, as it marks the beginning of the winter season in the Arctic region. During this month, the Arctic sea ice starts to freeze and form as the temperature drops. This process continues throughout the winter months, and by the end of winter, sea ice covers a large portion of the Arctic Ocean. The variation of sea ice near the land region makes one understand the land is yet to lose the heat it has absorbed during the summers. The land passes on its heat to the water nearby, causing the ice to melt away. As the latent heat capacity of water is quite high when compared to land/soil, the water tends to hold the heat for a prolonged period, which is thereafter passed to the nearby portions through the process of conduction with the help of wind and currents. This ultimately causes the ice to melt drastically. Recent winter warmings, when coupled with such transfer of heat (causing a decrease in albedo), inhibits the growth of sea ice. This prevailing situation not only hampers the growth of existing sea ice but also prevents the development of fresh ice.

During January (Figures 2d, 2e, and 2f), the range of SIC anomalies is seen shifting. The highest value is +80, and the lowest is -20. This clearly indicates that the recent fifteen years; 2006–2020 (Figures 2d, 2e, and 2f), have not gained sea-ice over the Barents as much as during the years 2001–2005. The contrast is somewhat similar to that during December, but here the anomaly has experienced a horizontal shift (the nearing of higher difference towards higher latitudes, more towards the Svalbard region). The region of the sea, south of Svalbard and north of Novaya Zemlya, experiences tremendous sea ice loss. Even the region south of Barents shows a huge contrast that was not observed during December, especially the area around Kolguyev island, over the White Sea, and around the Kanin Peninsula. During 2011–2015 (Figure 2e), the contrast remained similar, with little intensification around the islands of Svalbard and Novaya Zemlya. Sections over the Arctic Circle are also found to have positive anomalies, meaning the base period, 2001–2005, had more sea ice compared to 2011–2015. The lateral (spatial) spread of positive differences in SIC is greater during this period. By 2016–2020 (Figure 2f), the contrast reaches up to +80 near the northwest and southeast sectors of the sea. The plot during this span is extremely alarming, as nowhere over the sea has there been a visible effort by the atmospheric conditions to promote the growth of sea ice. The incapability of the atmospheric environment to favour the development of sea ice may be potentially due to the development of sea level pressure patterns in January. Researchers have already confirmed that the variation or the developments of such pressure patterns are due to changes in moisture which occur due to atmospheric transport from remote areas other than the Arctic (Zhao et al., 2022). Unlike December and January, February shows a different behaviour. The values from 2006 to 2010 (Figure 2g) were found to be significantly lower than those from 2001 to 2005. However, as the years progressed to 2011–2015, the differences were found to be less (Figure 2h) than they were between 2001 and 2005. However, as the years passed to reach 2011–2015, the difference was found to be less. And finally, by 2016–2020 (Figure 2i), the sea has lost tremendous amount of concentration, making the early years, 2001–2005, higher in value. February is typically one of the coldest and snowiest months in the region, and SIC is generally at its highest during this time. However, there has been a significant decline in Arctic SIC in recent years due to climate change and other factors. This decline has also affected the Barents Sea, and the sea ice concentration may vary from year to year depending on these factors.

In most cases, the timeline of sea ice melt is determined by whether the circulation patterns are strong or weak. March has always been a key period in the lifecycle of sea-ice growth. This month has the highest percentage of SIC in the sea ice life cycle during all the considered years. During 2006-2010 (Figure 2j), the contrast in SIC is similar to that during January, except for the fact that the south portion of the sea does not experience much difference, e.g., the White Sea. However, the area near Novaya Zemlya Island is seen to develop extreme

anomalies (positive) with the passage of years. By 2011–2015 (Figure 2k), SIC shows significant variation in positive anomalies to the east of Svalbard and Novaya Zemlya. By 2016–2020 (Figure 2l), the existing fluctuation is seen deepening. Overall, majority of the sea remains within the ~0 anomalies, stating that the years 2006–2020 are not much different from 2001–2005 in the formation or decay of sea-ice over the Barents Sea. March is often depicted as the winter peak month. Though recently it has been known that winter warming is quite high compared to summers. It is recorded that almost 50% of sea-ice reduction occurred in the month of March from 1979–2020. Additionally, during this month, significant ocean heat transport at the Barents is observed (Wang et al., 2019). Large amounts of heat get transported to the Barents Sea by Atlantic waters and by the Norwegian coastal current inflows. Unlike other months that have been discussed so far (December, January, February, and March), during April the scenario is different. The entire sea experiences an anomaly greater than zero. The entire west of Novaya Zemlya experiences a contrast. This variation is further observed near Kolguyev Island, the Kanin Peninsula, and also over the White Sea with the passage of time. Additionally, during 2006–2010, the area around Svalbard is found to be extremely devoid of any major anomalies. In fact, the south of the island experiences some negative anomalies ranging ~-15 proving that the years 2006–2010 have seen some development of sea ice when compared to the years 2001–2005. By 2011–2015, the constant was noticeable around Svalbard but not extremely significant. However, the west boundary of Novaya Zemlya is seen to intensify SIC to a greater extent. By 2016–2020, this depth of anomaly/variability will have further thickened. It is understood from the plots that the sea did not experience a favourable situation during the successive years for the ice to grow.

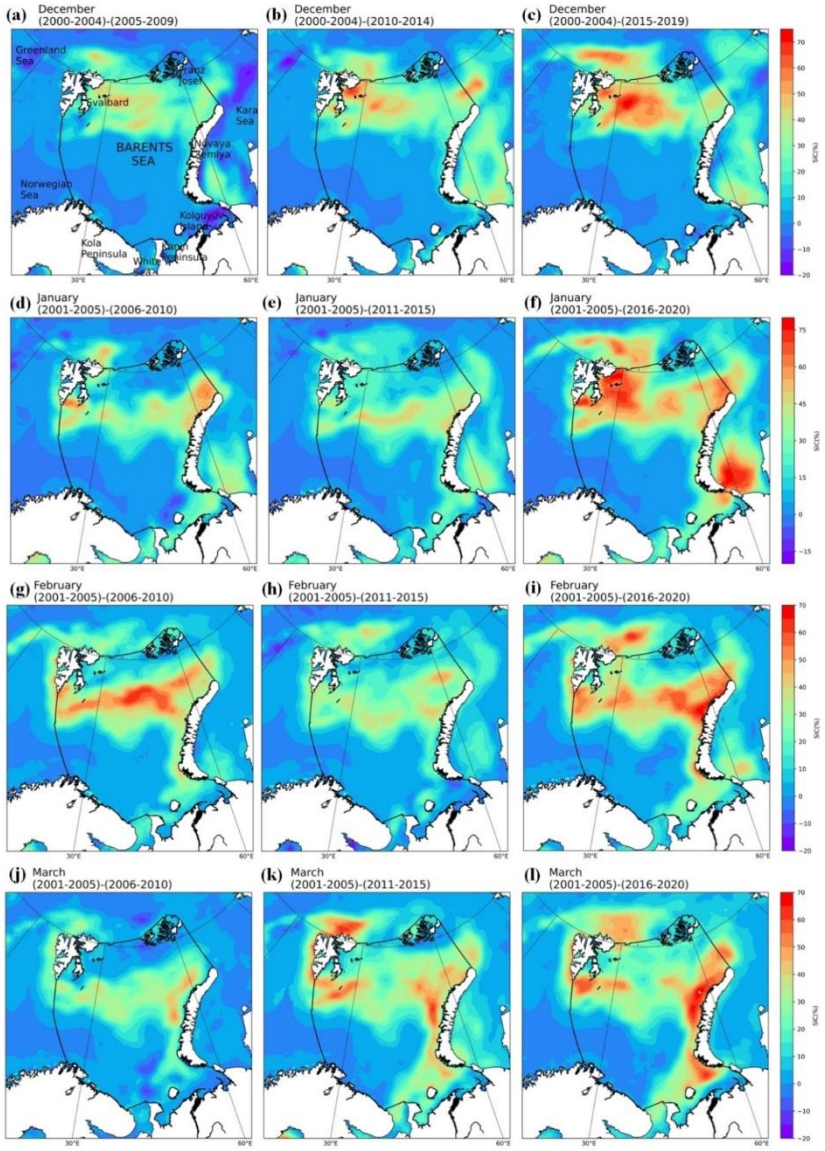

Figure 2. Spatial anomaly of SIC over Barents Sea during December in 2005-2009, 2010-2014, and 2015-2019 during a), b) and c) December d), e), and f) January g), h), and i) February j), k), and l) March

The whisker plot (Figure 3) illustrates the variation in the life-cycle of SIC over the Barents Sea during the span of 2000–2020. The range of SIC lies between 0 and 70%. As observed over the Arctic Sea, the Barents Sea also experiences its minimum sea-ice condition during September (highlighted in pink) and maximum during March (highlighted in blue). Months: April–September can be demarcated as the decay phase and October–March as the growth phase of sea ice. The diamond dots in the graph illustrate outliers, which are greatly observed during the decay process. The range during April is fairly broad, with a mean greater than 40%. The wideness in the range of SIC is seen to be decreasing thereafter. Correspondingly, the mean value is also found to be dropping. By June, the drop in SIC is significant, with the range falling below 10% by the month of September. The range, median, and mean are the lowest for this month, which is as expected. After September, SIC is seen to gradually build up. By December, the range in SIC is seen to be highly fluctuating, covering a wide range of concentrations. Soon in January, the median and mean values of SIC are seen to be greater than those during December; however, there is no noticeable incline in the range of SIC. Nevertheless, during January and also during February, the median remained the same. This indicated that during both months the values were almost the same, which divided the distribution between the lower half and the higher half. By March, which is also known as winter maxima, the median and mean are at their highest.

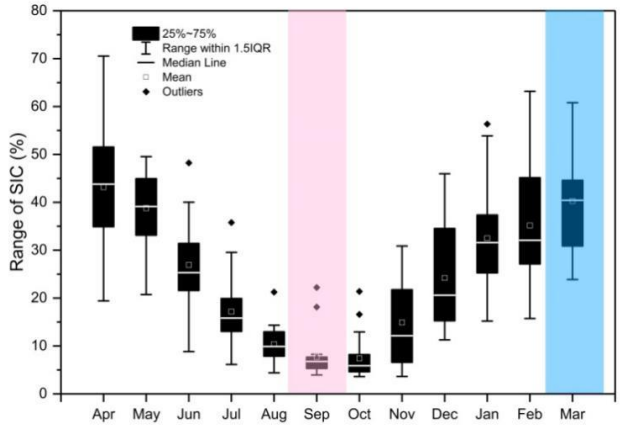

Figure 3. Temporal variability of SIC over the Barents Sea during summer (April-September) and winter (October-March) for the span of 2000-2020

3.2 Spatio-temporal variations of monthly SIT over Barents Sea

The spatial anomaly plot over Barents demonstrates the difference in SIT averages of 2016–2020 from 2011–2015. Unlike the anomaly plot of SIC, where two decades were divided into quadrants of five years each, in this case, the span is limited to 2011–2020 due to the unavailability of SIT data. From the anomaly plot, the general observation noted is that the central region of the Barents Sea remains devoid of many fluctuations (the range within zero). During December (Figure 4a), the horizontal section connecting Svalbard and Franz Josef is observed to have a positive anomaly of +0.35 m, stating that the years 2010–2014 had more SIT compared to that during 2015–2019. Additionally, the region west of Kara also experiences a difference. However, it is clearly evident that the south of Barents Sea remains devoid of any contrast, meaning the thickness has remained almost the same during the considered span over the region. By January (Figure 4b), the difference that had been observed around Svalbard during December had now intensified. The southeast corner of Novaya Zemlya also shows a variation, meaning all these places have lost tremendous ice during January 2016–2020. Even though it is alarming to notice that high positive anomalies are observed over the Arctic region, by February (Figure 4c), the entire east side of the Barents Sea had lost excessive sea ice. Kolguyev Island and the Kanin Peninsula, along with a few sections of the Arctic Circle, now show fluctuations. Regions at higher latitudes show positive anomalies, indicating that the sea gains back its lost thickness during 2016–2020. March (Figure 4d), which is also known as the month with maximum SIT, shows an equal contribution of both positive and negative anomalies. The inner sea consists of more positive values, whereas the outside of it has more negative values. The peripheral changes will definitely contribute to the sea making more sea ice. Therefore, by April, the sea had more negative anomalies. This clearly indicates that during April 2016–2020 (Figure 4e), the thickness of sea ice was definitely more compared to that during 2011–2015. However, by May (Figure 4f), the region closer to the land area—Svalbard, Franz Josef, Kolguyev Island, etc.—had gradually experienced positive values. From the plots, it can be substantiated that during 2016–2020, during the onset of winter (December, January, and February); the sea could not build up ice that was lost during summers. In March, April, and May, significant improvement is seen during the span. The probable reason might be the role played by atmospheric forcing, which has acted in favour of sea-ice growth. Still, it can be overlooked that the growth is quite low and hardly reaches 1 m. All the negative anomalies over the sea fall within the range of -0.35 to -0.25 m. The values are very low when compared to the ice, sea losses. However, in the larger picture, such small development in SIT can add a lot of importance to the cryospheric conditions over the region.

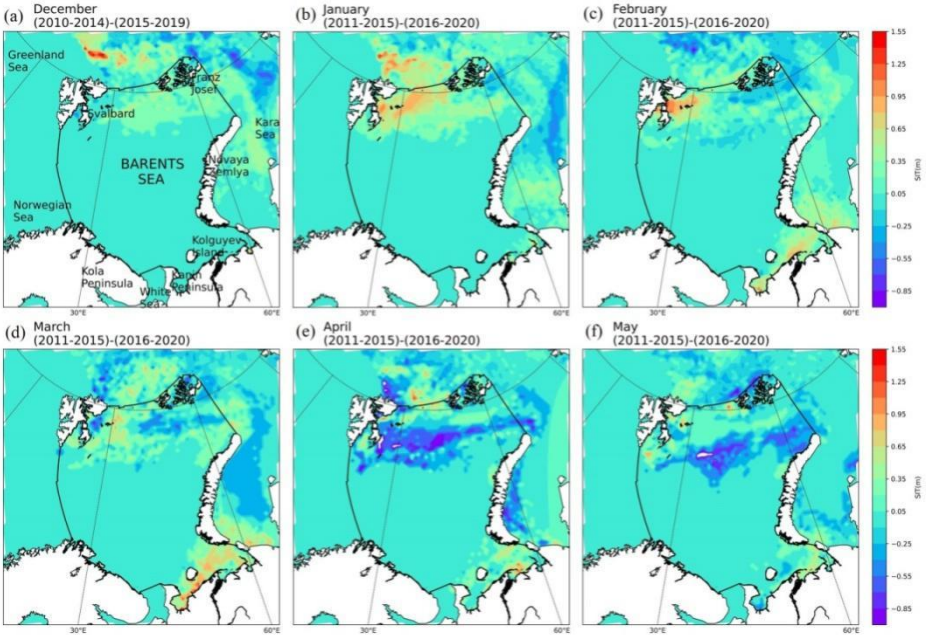

Figure 4. Spatial anomaly of SIT over Barents Sea during a) December b) January c) February d) March e) April and f) May 2010-2020

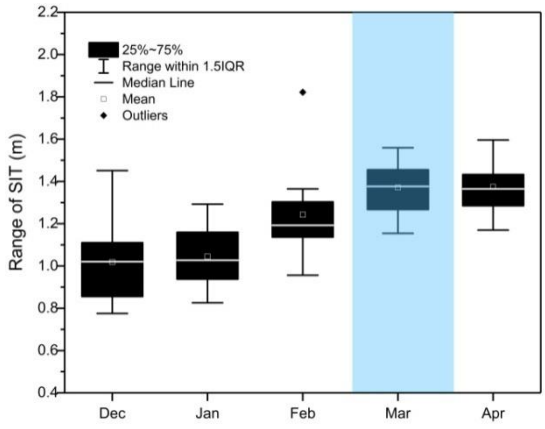

Figure 5. Temporal variability of SIT over the Barents Sea during December-May for the span 2010-2020

The temporal variation in SIT over the Barents Sea is depicted in Figure 5. The range over the sea varies between 0.7 and 1.6 m, including some outliers that go beyond 1.6 m. The plot clearly shows how the range increases as the winter months progress. The winter maximum is observed in the month of March. However, in Figure 5, the range during March and April seems to be almost the same, indicating that the developed thickness could not vanish away immediately with the onset of summer. Even the median in March is found to be higher than that in April. This indicates that the majority of pixels will have higher values of SIT during the next month. SIT data during the summer months is not available, therefore the transformation of the sea ice during those periods could not be observed. Anyway, the trend of its decay would be very similar to that of SIC, which has already been understood in the previous section.

3.3 Variability in Sea Ice Concentration with respect to Sea Ice Thickness

The histogram plot of SIC in Figure 6a has a range of 87–97%. Here the SIC values are obtained by averaging the data over all the years of each pixel of the respective month. For example, if we consider January, all the SIC values of January months are combined (averaged) for 2010–2020 (11 years), and later they are binned at 70 counts. The outputs obtained are displayed in Figure 6a. From the plot, it is evident that during January, February, and March, the lines overlap with each other. During January, SIC is observed to have a low percentage compared to the other two winter months, February and March. Due to the binning applied to the variable (SIC), the maximum count observed is ~5. However, the SIT plot (Figure 6b) shows a significant rise in thickness by a value of ~0.5 m with the passage of each month. The range of SIT here lies between 0.2 and 3.5 m. Figure 6b represents two Y axes, with one Y axis denoting the number of points (counts) having a particular thickness, the other Y axis showing the density of SIT, and the X axis representing SIT in metres (m). The density plot here represents the distribution of SIT. The highest peak, with a thickness of 1.2 m, is obtained in January.

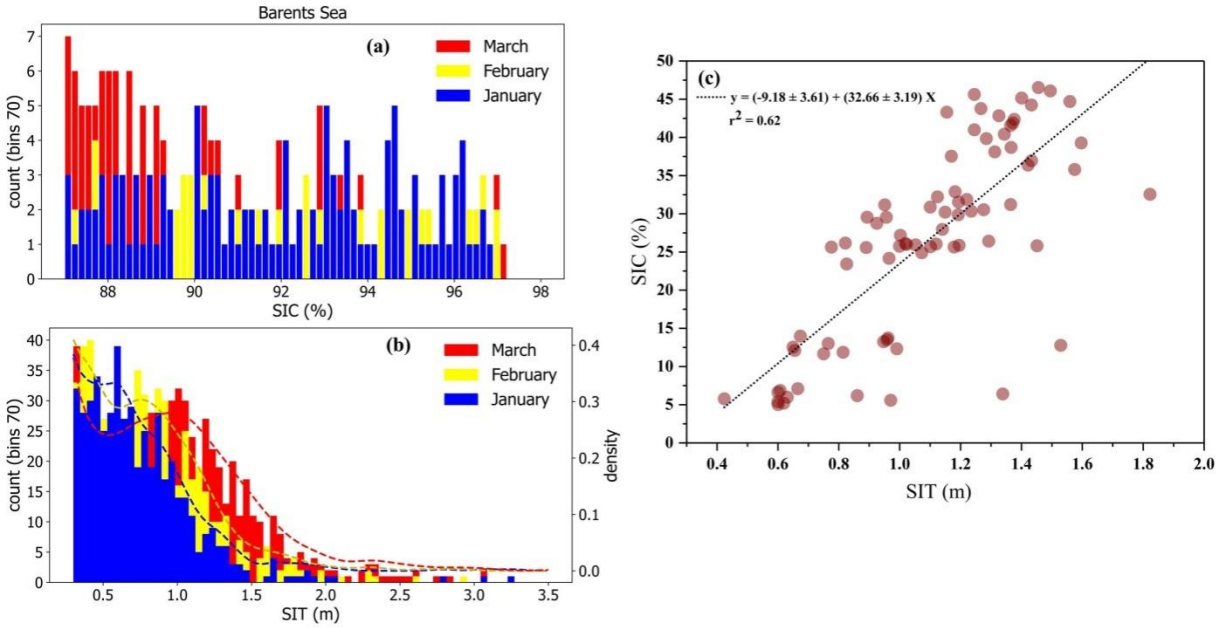

Figure 6. Histogram of a) Sea Ice Concentration and b) Sea Ice Thickness during January, February and March and c) Linear regression analysis of Sea Ice Concentration (SIC) with respect to Sea Ice Thickness (SIT) over Barents Sea during winter months (October-April) for the span 2010-2021

During February, the maximum peak slightly shifts to attain the value of 1.5 m. The shift in peak helps one understand the increase in the depth of sea ice, which is obtained as a result of favourable conditions (especially during winters). Furthermore, the highest value had fallen to 1.7 m by March. Here, the density distribution during January and February is observed to be almost the same, which is thereafter followed by a slight decline during March. It is worth noting that the SIT of about 2 m in March over the Barents Sea is seasonal. FYI or MYI refers to thick ice greater than 2 m in thickness. In the analysed plots displayed in Figure 6a, the frequent appearances of SIC within the range of 90–100% are seen to be in proper agreement with the shift of thick sea ice (Figure 6b).The winter monthly variation of SIC with respect to SIT over Barents for the span of 11 years is illustrated in Figure 6c. From the plot, it is evident that the range of SIC varies between 0-50 % and that of SIT varies between 0.2-2m. SIT and SIC own a high linear correlation and also have noticeable seasonal variation characteristics. When SIC increases, SIT also increases, and vice versa. Over the Barents Sea, the $r^2_{(SIC, SIT)} = 0.62$ ($p < 0.05$), indicating a strong relationship between the two quantities.

3.4 Numerical Logistic Curve Model

3.4.1 Logistic SIC decay process averaged over summer months (April-September)

From the literature, it is clearly evident that atmospheric changes highly influence the development of cryospheric features (e.g., Qin and Ding, 2010). The Earth's climate system is a complex and dynamic system, and changes in one component can have far-reaching effects on others, thereby influencing the sea ice conditions. This underscores the importance of understanding and monitoring the entire system to accurately predict future trends and mitigate the impacts of climate change. However, here, the work revolves around understanding the standard numerical logistic curve model for predicting the fate of sea-ice conditions. Figure 7 shows the decay of sea ice during the summer months, i.e., from April to September. The time series of model-predicted SIC and satellite-observed SIC is drawn so as to understand the closeness of these parameters. The predicted SIC is calibrated by the numerical formula of the logistic curve model using the methodology discussed in the aforementioned section. From the visual observation, it is clearly evident that the calculated b matches well with the satellite-derived SIC.

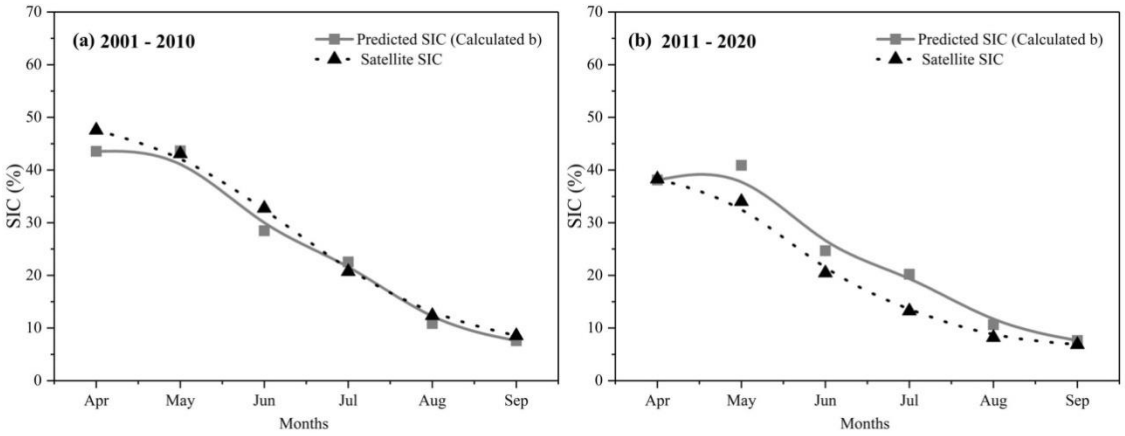

Figure 7. Temporal variability of SIC over Barents Sea during summer (April-September) for the span a) 2001-2010 and b) 2011-2020.

For the years 2001–2010 (Figure 7a), it is seen that the predicted SIC is seen to overlay with satellite data for several months. Apart from that, the percentage difference is calculated to understand the extent of the difference between the two SICs. Here, points during April, May, and July are an exact match. The percentage difference between the predicted SIC for these three months and the satellite-derived SIC is found to be 8.82%, 1.27%, and 8.49%, respectively. The highest difference between the values was noted in the month of June (13.98%), which is not significantly visible in Figure 7. However, the predicted SIC clearly shows the summer life cycle of SIC. It is highest in the month of April, with a range of 50–40%, and gradually declines by September, which is also recorded as the month of sea-ice minimum. However, the regression analyses performed in the subsequent sections add to our understanding of the method and its closeness to the satellite-drawn observations. During the recent decade, 2011-2020 (Figure 7b) predicted SIC and satellite SIC are seen to line up well with each other, as in the case of 2001-2010 (Figure 7a). The two datasets clearly show the decay of sea ice from April to September. April is the month with the highest value, and September is the month with the lowest value, which is the existing trend of sea ice over the region during the summer phase. Figure 7b shows the real scenario prevailing over the region, with the highest difference between the two SICs in the month of July and the lowest in August. The highest closeness was observed at 0.49% in the month of August. The match between the starting and ending values of the sea ice decay life cycle clearly demonstrated that the trend could be correctly determined to a greater extent well in advance. The highest difference between the two was with value reaching 41.73% in the month of July. The difference observed in this case is phenomenally high, which might be due to other atmospheric forcings that are not currently incorporated in the numerical logistic curve equation. July, being the mid-month of summer, might have experienced tremendous warming during the recent decade, which has made the sea undergo significant melting beyond the predicted decay. During May and June, the match between the two values was also high, with values of 18.35% and 18.68%, respectively. August also has the second-largest SIC difference, with 25.90%. Figure 7 clearly states that during this period, the predicted SIC works fine over the region.

3.4.2 Logistic SIC decay process averaged over winter months (October-March)

Similar to the summer months (Figure 7), the standard logistic curve is also applied to the winter months (Figure 8). Sea ice grows from October to March, with the maximum amount occurring in March. From Figure 8, it is evident that during both decades, predicted SIC is in line with satellite-obtained SIC except for few differences during few months. During the growth stage (winter phase), the lowest range of SIC (minimum SIC) is observed in the month of October and the maximum in the month of March. In Figure 8a, the predicted SIC is found to show the highest similarity with the satellite SIC during March and December, with a percentage difference of just 2.98% and 4.62%, respectively, between the two. However, the largest difference between the two quantities was seen during the month of November, with a percentage dissimilarity of 32.59%, which is not quite high but the highest amongst all the other winter months. Further, the second largest difference between the two SICs is observed in the month of February with a value of 12.00%, followed by January with a value of 10.61%.

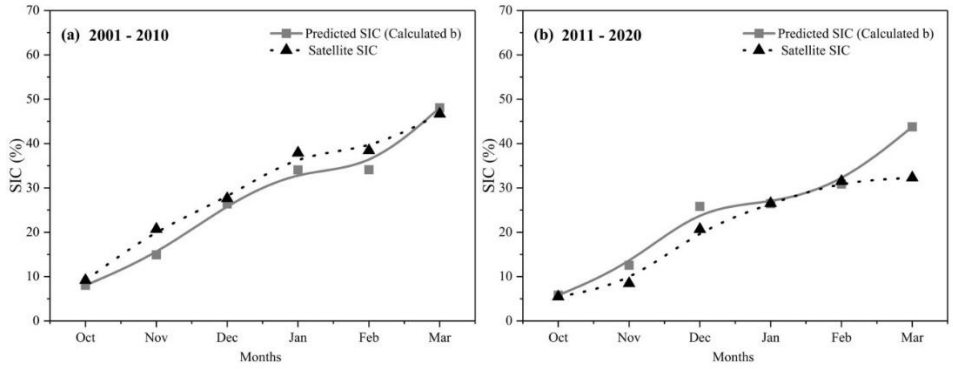

Figure 8. Temporal variability of SIC over Barents Sea during winter (October-March) for the span a) 2001-2010 and b) 2011-2020.

During the recent decade 2011–2020 (Figure 8b), the trend line of the predicted SIC is seen to match well with the satellite-obtained SIC. This nature of the time series during this decade indicates that the predicted SICs can be used to know the health of sea ice well in advance. However, the percentage differences between predicted SIC and satellite SIC is more during this span than during the previous span (2001–2010). The difference between the two SICs is the smallest during October, January, and February, with values of 5.97%, 0.31%, and 1.97%, respectively. For all the other months, the percentage difference is quite higher than 10%. However, here also, the highest is observed in the month of November, with a value of 38.97%. Apart from Figures 6 and 7, which give a visual interpretation of the closeness of SICs, regression analyses in the upcoming section provide a better understanding of the calibration of the standard logistic curve model in predicting the cryospheric variable, SIC.

3.4.3 Regression analyses between predicted and satellite SIC during summer and winter months

In order to validate the efficacy of the standard logistic curve during summer when sea ice undergoes decay, regression analyses are performed between the predicted SIC and satellite SIC, and the results are displayed in Figure 9. Similar to the previous section, where the model was applied over the span of each decade, i.e., 2001–2010 and 2011–2020, here too the regression analyses are performed on similar timelines. Figure 9 gives information about the closeness of the predicted and satellite-obtained SICs. The obtained coefficient of determination gives an understanding of the fit of predicted data with satellite-derived SIC. The calculation of the p-value here gives an understanding of the confidence level (in this case; 95%) that prevails between the two datasets. For years 2001–2010 (Figure 9a), r^2 = 0.88 between predicted SIC and satellite SIC. The coefficient of determination being greater than 0.5 indicates predicted SIC is significant with satellite SIC. Similarly, during the span of 2011–2020 (Figure 9b), the coefficient of determination is greater than 0.5, with r^2 = 0.87. The marginal difference between the two predicted SICs with the satellite SIC was low during the previous decade of 2001–2010 compared to the latter period of 2011–2020.

Similar to summers, in order to validate the functioning of the model during winter, regression analyses are performed between predicted SIC and satellite SIC. Here also, the coefficient of determination value during 2001–2010 (Figure 10a) reveals that the predicted value fits well with the satellite SIC. The r^2 value in the former case is 0.80 with level of significance $p<0.05$, indicating that the confidence level is greater than 95%. However, during 2011–2020 (Figure 10b), r^2 = 0.78 of the satellite SIC with the predicted SIC In this case, the range of r^2 is ~0.7, stating that the method can be adopted to determine SIC.

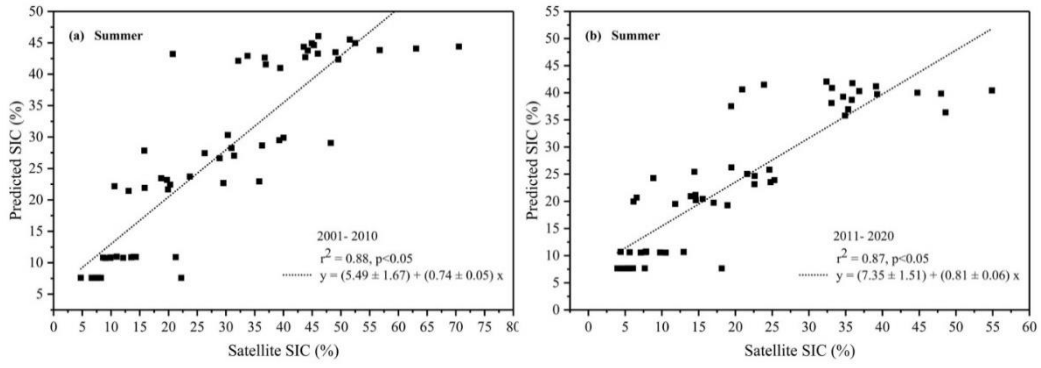

Figure 9. Correlation between predicted and satellite SIC during summer (April - September) for the span a) 2001-2010 and b) 2011-2020

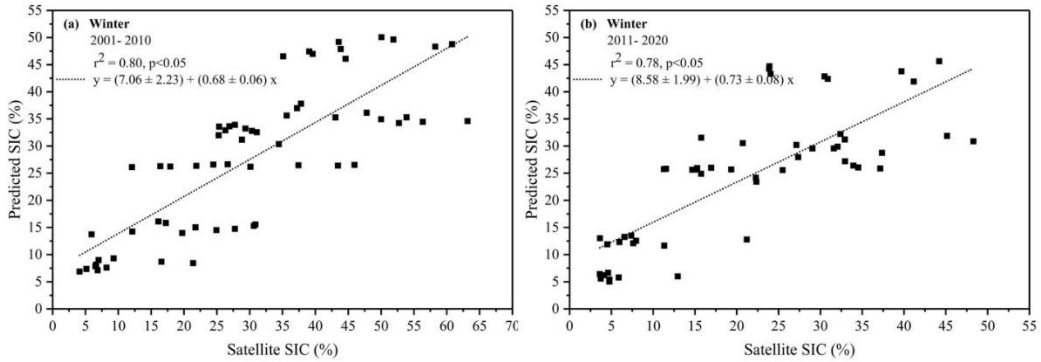

Figure 10. Correlation between predicted and satellite SIC during winter (October-March) for the span a) 2001-2010 and b) 2011-2020.

3.4.4 Evolution of SIT and regression analyses between predicted and satellite SIT during December – April

Apart from the implication of the logistic curve on the parameter SIC, we have tried to understand the further scope of this model by applying it to another sea-ice parameter, namely SIT. Looking at the general behaviour of thickness, the parameter is found to range between 0 and 2 m, which is also well noted in the aforementioned section. Here, however, the model-obtained SIT is tested with the satellite-derived SIT to understand the closeness of the derived SIT. In terms of the trend line, the predicted SIT exhibits similar patterns to that of satellite SIT, indicating that the model works well on this cryospheric parameter as well. Additionally, the degree of closeness in the predicted SIT is seen to be good compared to that of the satellite SIT. From Figure 11a, it is evident that October is the month with the lowest SIT and March–April with the highest. However, when observing the satellite SIT, it is clearly evident that March has the highest SIT; the SIT during March is greater than that during April. While with the predicted SIT, April is found to show the highest value, indicating the development of sea-ice growth even during the onset of summer. This information may be misleading at times. While checking the difference in the value between predicted SIT and satellite SIT, March and April had a difference of about 2.95% and 6.93%, respectively. The highest difference between the two SITs was observed in the months of November and December, with values of 21.17% and 19.42%, respectively. The difference in November is not much, which still indicates an appreciable match. Further computation of the percentage difference between the predicted SIT and the satellite-obtained SIT revealed that the majority of the values were insignificant. For the months of October, January, and February, the differences between the SITs were 13.06%, 16.35%, and 14.81%, respectively. Despite these differences between the two entities, the predicted values of SIT are more reliable.

After observing the trend followed by the predicted SIT, it is vital to validate the closeness of modelled data with satellite data. This is done by performing linear regression analyses between the predicted SIT and the satellite SIT. Figure 11b displays the results of analyses performed between these SITs during December and May for the years 2011–2020. From Figure 11b, $r^2 = 0.75$ for calculated SIT with satellite-derived SIT. The coefficient of determination values state that the calculated SIT matches well with the satellite SIT. From the above observations, it can be stated that the standard logistic curve model works fine for each month. Also, the model can be extended to incorporate more cryospheric parameters, as it is now proven that SIC and SIT work fine with the model.

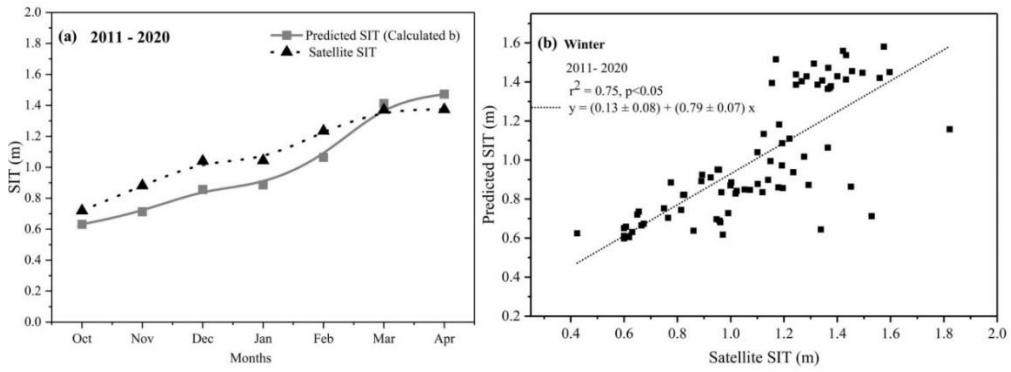

Figure 11. a) Temporal variability of SIT and b) correlation between predicted and satellite SIT over the Barents Sea during winter (October-April) for the span 2011-2020

4. Conclusions

With the recently discovered process of Atlantification taking place over the Arctic region, the marginal Barents Sea has now gained special attention from researchers, as this sea serves as a gateway for the Atlantic water to merge into the Arctic region. This study paves a new quantitative statistical approach for a better understanding of the seasonal sea ice processes. The statistical approach used here is the standard logistic curve model, which is proven to be an outstanding tool for both the summer and winter seasons. The sea ice patterns show high monthly variability over the Barents Sea. In general, the sea ice grows from mid-September to mid-March and decays from mid-March to mid-September. In order to understand the existing nature of sea ice, two cryospheric parameters namely SIC and SIT are considered. The SIC over the region is seen to peak in winter and decrease to its lowest in summer. During the considered period, the Barents SIC is seen decreasing 87–97% with the passage of time. However, the decline is better explained by the parameter, SIT. Additionally, SIT revealed that there is intensification in thickness with each month's shift. The peak of SIT shifts from 1.2 to 1.5 m during January and February and from 1.5 to 1.7 m during February and March. The standard logistic curve model is selected to quantify the sea ice growth and decay processes during the two seasons. For the summer months, the fitted SIC derived from the standard logistic curve model is in good consistent with the average satellite data every ten years (decade); 2001-2010 and 2011-2020. The rapid decline in the SIC pattern from mid-May to September is successfully characterized by the fitted (modelled) curves. For the winter months, the fitted SIC derived from the standard logistic curve model is in good dependence with the average true (satellite) data during the above-mentioned different time periods. The gradual increase in SIC from November to March is well reflected by these fitted curves. Further, mathematical validation of modelled obtained data is done with the satellite SIC with the help of regression analyses. The coefficient of determination (r^2) values obtained for predicted SIC and satellite SIC during summer for the years 2001-2010 and 2011-2020 are 0.88 and 0.87 respectively. Whereas during winter, these values correspond to 0.80 and 0.78 are for the above-mentioned years. Additionally, SIT is also predicted using this model. In this case, the duration is kept confined to December - April for the year 2011-20. During these months, the fitted SITs derived from the model are in good support with the average satellite data during the decade. The same has been proven mathematically by deriving the coefficient of determination (r^2) values between the predicted SIT and the satellite SIT. The correlation co-efficient value is 0.75 which is obtained between modelled SIT and satellite SIT for the months December - April for the years 2011-20. From the observations, it is clear that the model can be used to understand the state of sea condition to a large extent. This enhancement in the values is mostly due to considering individual ‘b’ values for each month, which compensates for the varying nature of sea ice features.

This study promotes the understanding of sea ice - both in the x-y plane; SIC and z-plane; SIT in the marginal - Barents Sea. The modelled results are not only seen to match with the satellite data but are also seen to yield good r^2 values, stating it can also be used to foresee the future scenario of the sea. Additionally, developing a numerical model like this helps in predicting sea ice behaviour well into the future. Additional development of the model by incorporating the external driving forces of sea ice - atmospheric and oceanic variables will help in accurately computing the future cryospheric conditions at the micro scale and macro scale. Future work may be to investigate more sea ice parameters using the same standard logistic curve model over different spatial and temporal domains.

References

ACIA - Arctic Climate Impact Assessment (2005). Arctic climate impact assessment - Scientific report. Cambridge University Press.

Allen MR, OP Dube, W Solecki, F Aragón-Durand, W Cramer, S Humphreys, M Kainuma, J Kala, N Mahowald, Y Mulugetta, R Perez, M Wairiu and K Zickfeld (2018). Framing and Context. In: Global Warming of 1.5°C. An IPCC Special Report on the impacts of global warming of 1.5°C above pre-industrial levels and related global greenhouse gas emission pathways, in the context of strengthening the global response to the threat of climate change, sustainable development, and efforts to eradicate poverty.

Bengtsson L, P Arkin, P Berrisford, P Bougeault, CK Folland, C Gordon, K Haines, KI Hodges, P Jones, P Kallberg, N Rayner, AJ Simmons, D Stammer, PW Thorne, S Uppala and RS Vose (2007). The need for a dynamical climate reanalysis. Bulletin of the American Meteorological Society, 88(4), 495-502. https://doi.org/10.1175/bams-88-4-495

Bitz CM and WH Lipscomb (1999). An energy-conserving thermodynamic model of sea ice. Journal of Geophysical Research: Oceans, 104(C7), 15669-15677. https://doi.org/10.1029/1999jc900100

Boé J, A Hall and X Qu (2010). Sources of spread in simulations of Arctic Sea ice loss over the twenty-first century. Climatic Change, 99(3-4), 637-645. https://doi.org/10.1007/s10584-010-9809-6

Bony S, R Colman, VM Kattsov, RP Allan, CS Bretherton, J Dufresne, A Hall, S Hallegatte, MM Holland, W Ingram, DA Randall, BJ Soden, G Tselioudis and MJ Webb (2006). How well do we understand and evaluate climate change feedback processes? Journal of Climate, 19(15), 3445-3482. https://doi.org/10.1175/jcli3819.1

Cavalieri DJ, CL Parkinson, P Gloersen, and HJ Zwally. (1996), updated yearly. Sea Ice Concentrations from Nimbus-7 SMMR and DMSP SSM/I-SSMIS Passive Microwave Data, Version 1. [sea ice thickness]. Boulder, Colorado USA. NASA National Snow and Ice Data Center Distributed Active Archive Center. https://doi.org/10.5067/8GQ8LZQVL0V [28/09/2021].

Cavalieri DJ and CL Parkinson (2012). Arctic Sea ice variability and trends, 1979–2010. The Cryosphere, 6(4), 881-889. https://doi.org/10.5194/tc-6-881-2012

Chen P and J Zhao (2017). Variation of sea ice extent in different regions of the Arctic Ocean. ActaOceanologicaSinica, 36(8), 9-19. https://doi.org/10.1007/s13131-016-0886-x

Danabasoglu G, JF Lamarque, J Bacmeister, DA Bailey, AK DuVivier and J Edwards (2020). The Community Earth System Model Version 2 (CESM2). Journal of Advances in Modeling Earth Systems, 12, e2019MS001940. https://doi.org/10.1029/2019MS001940

Diebold FX and GD Rudebusch (2020). Probability Assessments of an Ice-Free Arctic: Comparing Statistical and Climate Model Projections. Federal Reserve Bank of San Francisco Working Paper 2020-02. https://doi.org/10.24148/wp2020-02

Eisenman I and JS Wettlaufer (2008). Nonlinear threshold behavior during the loss of Arctic Sea ice. Proceedings of the National Academy of Sciences, 106(1), 28-32. https://doi.org/10.1073/pnas.0806887106

Holland MM, CM Bitz and B Tremblay (2006). Future abrupt reductions in the summer Arctic Sea ice. Geophysical Research Letters, 33(23). https://doi.org/10.1029/2006gl028024

Hui C (2006). Carrying capacity, population equilibrium, and environment's maximal load. Ecological Modelling, 192, 317-320.

Inoue J, ME Hori and K Takaya (2012). The role of Barents Sea ice in the wintertime cyclone track and emergence of a Warm-Arctic cold-siberiananomaly. Journal of Climate, 25(7), 2561-2568. https://doi.org/10.1175/jcli-d-11-00449.1

Intergovernmental Panel on Climate Change. (2018). Global warming of 1.5°C. An IPCC special report on the impacts of global warming of 1.5°C above pre-industrial levels and related global greenhouse gas emission pathways, in the context of strengthening the global response to the threat of climate change, sustainable development, and efforts to eradicate poverty. World Meteorological Organization.

Katlein C, S Arndt, M Nicolaus, DK Perovich, MV Jakuba, S Suman, S Elliott, LL Whitcomb, CJ McFarland, R Gerdes, A Boetius and CR German (2015). Influence of ice thickness and surface properties on light transmission through arctic sea ice. Journal of Geophysical Research: Oceans, 120(9), 5932-5944. https://doi.org/10.1002/2015jc010914

Kim B, S Son, S Min, J Jeong, S Kim, X Zhang, T Shim and J Yoon (2014). Weakening of the stratospheric polar vortex by Arctic sea-ice loss. Nature Communications, 5(1). https://doi.org/10.1038/ncomms5646

King JC and J Turner (1997). Antarctic Meteorology and climatology. Cambridge University Press. https://doi.org/10.1017/cbo9780511524967

King J, G Spreen, S Gerland, C Haas, S Hendricks, L Kaleschke and C Wang (2017). Sea-ice thickness from field measurements in the northwestern Barents Sea. Journal of Geophysical Research: Oceans, 122(2), 1497-1512. https://doi.org/10.1002/2016jc012199

Kurtz N and J Harbeck.(2017). CryoSat-2 Level-4 Sea Ice Elevation, Freeboard, and Thickness, Version 1. [sea ice thickness]. Boulder, Colorado USA. NASA National Snow and Ice Data Center Distributed Active Archive Center. https://doi.org/10.5067/96JO0KIFDAS8 [28/09/2021]

Kyurkchiev N and S Markov (2015). On the Hausdorff distance between the heaviside step function and Verhulst logistic function. Journal of Mathematical Chemistry, 54(1), 109-119. https://doi.org/10.1007/s10910-015-0552-0

Lind S, RB Ingvaldsen and T Furevik (2018). Arctic warming hotspot in the northern Barents Sea linked to declining sea-ice import. Nature Climate Change, 8(7), 634-639. https://doi.org/10.1038/s41558-018-0205-y

Meier WN, GK Hovelsrud, BE Van Oort, JR Key, KM Kovacs, C Michel, C Haas, MA Granskog, S Gerland, DK Perovich, A Makshtas and JD Reist (2014). Arctic Sea ice in transformation: A review of recent observed changes and impacts on biology and human activity. Reviews of Geophysics, 52(3), 185-217. https://doi.org/10.1002/2013rg000431

Meredith M, M Sommerkorn, S Cassotta, C Derksen, A Ekaykin, A Hollowed, G Kofinas, A Mackintosh J Melbourne-Thomas, MMC Muelbert, G Ottersen, H Pritchard and EAG Schuur (2019). Polar Regions. In: IPCC Special Report on the Ocean and Cryosphere in a Changing Climate.

Meyer P (1994). Bi-logistic growth. Technological Forecasting and Social Change, 47, 89-102.

Mundy C, D Barber and C Michel (2005). Variability of snow and ice thermal, physical and optical properties pertinent to sea ice algae biomass during

spring. Journal of Marine Systems, 58(3-4), 107-120. https://doi.org/10.1016/j.jmarsys.2005.07.003

Murphy H, H Jaafari and HM Dobrovolny (2016). Differences in predictions of ODE models of tumor growth: A cautionary example. BMC Cancer, 16(1). https://doi.org/10.1186/s12885-016-2164-x

Nghiem SV, Y Chao, G Neumann, P Li, DK Perovich, T Street and P Clemente-Colón (2006). Depletion of perennial sea ice in the east Arctic Ocean. Geophysical Research Letters, 33(17). https://doi.org/10.1029/2006gl027198

Notz D (2009). The future of ice sheets and sea ice: Between reversible retreat and unstoppable loss. Proceedings of the National Academy of Sciences, 106(49), 20590-20595. https://doi.org/10.1073/pnas.0902356106

Parkinson CL (2019). A 40-y record reveals gradual Antarctic sea ice increases followed by decreases at rates far exceeding the rates seen in the Arctic. Proceedings of the National Academy of Sciences, 116(29), 14414-14423. https://doi.org/10.1073/pnas.1906556116

Parkinson C L and DJ Cavalieri (2008). Arctic Sea ice variability and trends, 1979–2006. Journal of Geophysical Research, 113(C7). https://doi.org/10.1029/2007jc004558

Petty AA, MM Holland, DA Bailey and NT Kurtz. (2018). Warm Arctic, increased winter sea ice growth?. Geophysical Research Letters, 45(23). https://doi.org/10.1029/2018gl079223

Qin D and Y Ding (2010). Key issues on Cryospheric changes, trends and their impacts. Advances in Climate Change Research, 1(1), 1-10. https://doi.org/10.3724/sp.j.1248.2010.00001

Ren S, X Liang, Q Sun, H Yu, LB Tremblay, B Lin, X Mai, F Zhao, M Li, N Liu, Z Chen and Y Zhang (2021). A fully coupled Arctic sea-ice–ocean–atmosphere model (ArcIOAM v1.0) based on C-Coupler2: model description and preliminary results. Geoscientific Model Development, 14(3), 1529-1556. https://doi.org/10.5194/gmd-14-1529-2021

Rösel A, P Itkin, J King, D Divine, C Wang, MA Granskog, T Krumpen and S Gerland (2018). Thin sea ice, thick snow, and widespread negative Freeboard observed during N-ICE2015 north of Svalbard. Journal of Geophysical Research: Oceans, 123(2), 1156-1176. https://doi.org/10.1002/2017jc012865

Schlichtholz P (2019). Subsurface ocean flywheel of coupled climate variability in the Barents Sea hotspot of global warming. Scientific Reports, 9(1). https://doi.org/10.1038/s41598-019-49965-6

Schröder L, M Horwath, R Dietrich and V Helm (2018). Four decades of surface elevation change of the Antarctic ice Sheetfrom multi-mission satellite altimetry. https://doi.org/10.5194/tc-2018-49

Screen JA, C Deser, DM Smith, X Zhang, R Blackport, PJ Kushner, T Oudar, KE McCusker and L Sun (2018). Consistency and discrepancy in the atmospheric response to Arctic sea-ice loss across climate models. Nature Geoscience, 11(3), 155-163. https://doi.org/10.1038/s41561-018-0059-y

Serreze MC, MM Holland and J Stroeve (2007). Perspectives on the Arctic's shrinking sea-ice cover. Science, 315(5818), 1533-1536. https://doi.org/10.1126/science.1139426

Shapiro I, R Colony and T Vinje (2003). April sea ice extent in the Barents Sea, 1850–2001. Polar Research, 22(1), 5-10. https://doi.org/10.3402/polar.v22i1.6437

Simonsen K and PM Haugan (1996). Heat budgets of the Arctic Mediterranean and sea surface heat flux parameterizations for the nordic seas. Journal of Geophysical Research: Oceans, 101(C3), 6553-6576. https://doi.org/10.1029/95jc03305

Skagseth Ø, T Eldevik, M Årthun, H Asbjørnsen, VS Lien and LH Smedsrud (2020). Reduced efficiency of the Barents Sea cooling machine. Nature Climate Change, 10(7), 661-666. https://doi.org/10.1038/s41558-020-0772-6

Smedsrud LH, I Esau, R Ingvaldsen, T Eldevik, P Haugan, C Li, V Lien, A Olsen, A Omar, O Otterå, B Risebrobakken, A Sandø, V Semenov and S Sorokina (2013). The Role of the Barents Sea in the Arctic Climate System. Reviews of Geophysics, 51, 415-449.

Sorokina SA, C Li, JJ Wettstein and NG Kvamstø (2016). Observed atmospheric coupling between Barents Sea ice and the Warm-Arctic cold-siberian anomaly pattern. Journal of Climate, 29(2), 495-511. https://doi.org/10.1175/jcli-d-15-0046.1

Stroeve J and WN Meier (2018). Sea Ice Trends and Climatologies from SMMR and SSM/I-SSMIS, Version 3. [sea ice concentration]. Boulder, Colorado USA. NASA National Snow and Ice Data Center Distributed Active Archive Center. https://doi.org/10.5067/IJ0T7HFHB9Y6. [28/09/2021].

Sweilam NH, MM Khader and AM Mahdy (2012). Numerical studies for fractional-order logistic differential equation with two different delays. Journal of Applied Mathematics, 2012, 1-14. https://doi.org/10.1155/2012/764894

Tietsche S, D Notz, JH Jungclaus and J Marotzke (2013). Assimilation of sea-ice concentration in a global climate model – physical and statistical

aspects. Ocean Science, 9(1), 19-36. https://doi.org/10.5194/os-9-19-2013

Tronstad S, O. Pavlova and R Ingvaldsen (2007). Havklima (marine climate), in Forvaltningsplan Barentshavet. 1. Rapport fra overva˚kingsgruppen, edited by K. Sunnana˚, Chapter 4.1., pp. 12 – 15, Inst. Mar. Res., Bergen, Norway.

Turner J, GJ Marshall, K Clem, S Colwell, T Phillips and H Lu (2019). Antarctic temperature variability and change from station data. International Journal of Climatology, 40(6), 2986-3007. https://doi.org/10.1002/joc.6378

Vázquez M, R Nieto, A Drumond and L Gimeno (2016). Extreme sea ice loss over the Arctic: An analysis based on anomalous moisture transport. Proceedings of the 1st International Electronic Conference on Atmospheric Sciences. https://doi.org/10.3390/ecas2016-d003

Vella D and JS Wettlaufer (2008). Explaining the patterns formed by ice floe interactions. Journal of Geophysical Research, 113(C11). https://doi.org/10.1029/2008jc004781

Walsh JE, WL Chapman and F Fetterer (2017). Sea ice extents continue to set new records: Arctic, Antarctic, and global results. EOS, Transactions American Geophysical Union, 98. https://doi.org/10.1029/2017eo068607

Wang M and JE Overland (2009). A sea ice free summer Arctic within 30 years? Geophysical Research Letters, 36(7). https://doi.org/10.1029/2009gl037820

Wang Q, X Wang, C Wekerle, S Danilov, T Jung, N Koldunov, S Lind, D Sein, Q Shu and D Sidorenko (2019). Ocean heat transport into the Barents Sea: Distinct controls on the upward trend and Interannual variability. Geophysical Research Letters, 46(22), 13180-13190. https://doi.org/10.1029/2019gl083837

Yang S and JH Christensen (2012). Arctic Sea ice reduction and European cold winters in CMIP5 climate change experiments. Geophysical Research Letters, 39(20). https://doi.org/10.1029/2012gl053338

Zhang J, DA and Rothrock (2003). Modeling global sea ice with a thickness and enthalpy distribution model in generalized curvilinear coordinates. Monthly Weather Review, 131(5), 845-861. https://doi.org/10.1175/1520-0493(2003)131<0845:MGSIWA>2.0.CO;2

Zhao J, D Barber, S Zhang, Q Yang, X Wang and H Xie (2017). Record low sea-ice concentration in the central Arctic during summer 2010. Advances in Atmospheric Sciences, 35(1), 106-115. https://doi.org/10.1007/s00376-017-7066-6

Zhao X, K Huang, JS Fu and SF Abdullaev, S. F. (2022). Long-range transport of Asian dust to the Arctic: Identification of transport pathways, evolution of aerosol optical properties, and impact assessment on surface albedo changes. Atmospheric Chemistry and Physics, 22(15), 10389-10407. https://doi.org/10.5194/acp-22-10389-2022